An Integration Scheme for Biomedical CT Image Segmentation*

X. M. Pardo[1], D. Cabello[1] and J. Heras[2]

[1] Dept. Electrónica e Computación
[2] Servicio de Cirurxía Ortopédica, Complexo Hospitalario Universitario
Universidade de Santiago de Compostela, Galicia, Spain

The 3D reconstruction of bones is very useful in medical applications such as presurgical planning of prosThesis implant. A vital step in the geometrical modeling of the bone/implant interface is the bone segmentation, which, usually needs a lot of human interaction. In order to release the surgeon from this tedious work, a robust segmentation system is needed. As noted by some authors, the integration of information from different segmentations could give robustness to this process. Here, an automatic integration method for the problem of delineating the contours of bone structures is presented. The system will integrate the classification information obtained from two segmentation methods, one based on region growing and the other based on snakes, using a Markov random field model.

Keywords: segmentation, computed tomography (CT), Markov Random Field, integration, optimization.

1. Introduction

The representation of the 3D shape of bones is a prerequisite in certain computer-aided medical procedures; e.g., the presurgical planning of prosthesis implant, where the accuracy of the geometrical model is crucial for the custom prosthesis design and the prediction of the evolution of the bone/implant interface (Keyak et al., 1993; Müller and Rüegsegger, 1995; Dario et al., 1996; Aritan et al., 1997;). The use of computational techniques allows good precision and repeatability, which improve the objectivity of measurement of shape parameters with respect to the manual segmentations.

The objective of this work is to develop an automatic system for the 3D segmentation of the tibia in a set of CT images in order to generate a surface model. The accuracy of the analysis strongly depends on the precision with which the geometry of the structure is defined. Many methods proposed in the literature for medical image segmentation are either edge-based or region-based approaches, that require a large interaction with the user for the control and correction of the results (Pepino et al., 1993; Müller and Rüegsegger, 1995; Brown et al., 1997). Both, region-based and edge-based methods, present advantages and disadvantages. Although noise affects any image processing algorithm, the region-based methods present less sensitivity than those based on the gradient. The same occurs with the loss of information at high frequency. On the contrary, the shape variations are better handled by means of a scheme based on contours. Furthermore, since the edge-based methods depend more on the changes in the gray levels than on the values of such gray levels, they are less sensitive to the distributions of the gray scales. The edge-based methods provide, in general, better location of the border between segments of a partition.

Knowledge can be incorporated into the segmentation process to produce better results; rule-based systems, for example, have been widely used to segment medical imagery (Dhawan and Arata, 1991; Sonka et al., 1996). Generally, the objective of these methods is the identification of structures more than its correct segmentation. On the other hand, the contour-based methods that are presently receiving the most attention are the deformable contours or

* This work was supported by Xunta de Galicia under Grant PGIDT99PXI20606B

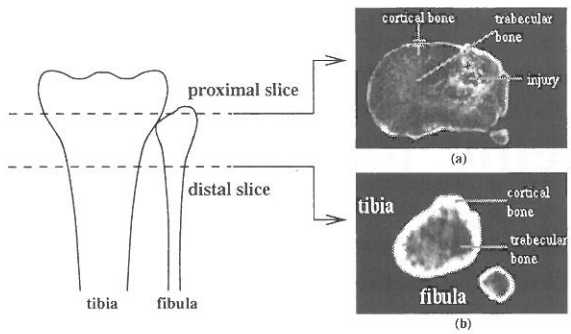

Fig. 1. Scheme of low knee bones: (a) cross section close to the proximal end; (b) cross section close to the distal end.

snakes (Kass et al., 1988). They also introduce knowledge into the segmentation process through the initial contour and the definition of the energy terms. In contrast to edge-based methods that first identify edges and then try to construct a closed boundary from the edges, this approach shapes an initial contour to match the boundary of the object.

A drawing identifying tibia, fibula, cortical bone and trabecular bone can be seen in Fig. 1, with the characteristics of the knee CT images. The width and the high density of the cortical bone and also the clear separation between tibia and fibula, Fig. 1b, make the segmentation of the tibia in the distal part fairly easy. As we approach the proximal part of the tibia, the thickness of the cortical bone decreases and the distance from the fibula is reduced. Moreover, problems of bone loss, cortical bone narrowness, malformations, etc., can be found. This leads up to: poorly defined bone external contours, little separation between the internal and external contour of the cortical bone and the proximity between contours of different structures, Fig. 1a. These characteristics imply several problems in the application of snakes. Some of these are: (1) existence of noise and/or textures in the background or inside the structures (trabecular bone), (2) very little distance between different structures, and (3) the existence of double contours (cortical bone). In these situations the contour can be trapped by spurious edge points. This makes the final result very sensitive to the initial conditions. For a correct delineation of the contour, the adjustment to the external part of the cortical bone is of paramount importance. When sequences of slices are being processed, the final contour in each slice can be used as the initial contour in the next slice. Serious approximation problems arise when injuries or deformations appear. In this case the initial contour can be located close to the internal contour of the cortical bone, and become trapped by it. Although the deformable contour models have demonstrated a great efficiency in the segmentation of biomedical structures, they are not limitation free. They continue to suffer dependency problems with the initial conditions. The majority of these algorithms can handle objects with simple geometry and topology, but they are often inadequate for objects with deep cavities and for structures made of different tissues (McInerney and Terzopoulos, 1995). These drawbacks appear frequently when treating bone structures with injuries.

On the other hand, the characteristics of knee CT images also lead the region-based methods to present problems. These include the inability of separating very close bone structures, the dislocation of bone contours and the undetection of the very thin cortical bone. Region-based systems present the advantage of having less sensitivity to noise. Its disadvantages reside in the difficulty of introducing shape information into the region growing process and in that the change of the pixel characteristics suggesting the presence of a contour can remain diluted in the global character of the region features. This frequently provokes undesired merging of regions. This infrasegmentation can be palliated with a division process that takes information from a border map. However, in injury zones or zones with very close structures, the border information can result incomplete. This is owed to the effect of interference between neighboring real transitions, and could make performing of a precise division impossible.

As noted by some authors, integration of information from different segmentations could give robustness to the segmentation process (Pavlidis and Liow, 1990; Chu and Aggarwal, 1993; Chakraborty et al., 1996; Tek and Kimia, 1997). However, this integration has almost always been carried out by complex systems or systems with a large dependency on the used segmentation algorithms. The majority of these approaches are only effective in the case of homogeneous structures with respect to a certain feature, but not in the case of structures with several textured parts. Here, a method that integrates different cues for the contour delineation

of bone structures is presented. The system integrates classifications (partitions) obtained by two segmentation methods, one based on region growing (Pardo et al., 1995) and the other based on snakes (Pardo et al., 1997) using a Markov random field model. This statistical model imposes connectivity and smoothness constraints on desired segmentation by Gibbsian priors.

The work is structured in the following way: in section 2 the idea of the Markov Random Field model is described, in section 3 an overview of the used segmentation methods and of the integration process that we have developed are presented, and in section 4 the results and conclusions of the present work are shown.

2. Background on Markov Random Fields

Frequently, vision problems are formulated as optimizing criteria due to uncertainties in vision processes such as noise and ambiguities in the interpretation. Generally, an exact solution does not exist, and we have looked for an optimal solution that satisfies certain constraints. The Markov Random Field theory provides a mathematical basis to solve the problem of making global inferences using local information. It is used in labeling problems to establish probabilistic distributions of interacting labels (Li, 1995).

The labeling of a scene is specified in terms of a set of sites, $\mathcal{S}$, and a set of labels, $\mathcal{L}$. A site is generally a point in the Euclidean space like a pixel or a region. The labeling problem consists of assigning a label to each of the sites, $f : \mathcal{S} \rightarrow \mathcal{L}$. The sites in $\mathcal{S}$ are related to each other through a neighborhood system, this is defined as $\mathcal{N} = \{\mathcal{N}_i | \forall i \in \mathcal{S}\}$, where $\mathcal{N}_i$ is the set of sites neighboring in i.

The pair $(\mathcal{S}, N)$ constitutes a graph $\mathcal{G}$, where $\mathcal{S}$ contains the nodes and $\mathcal{N}$ determines the links between the nodes according to the neighboring relationship. The n-site *clique*, C_n, for $(\mathcal{S}, N)$, is defined as a subset of $\mathcal{S}$ which collections of n sites that are neighbors to one another.

Let $\mathcal{F} = F_1, \ldots, F_m$ be a family of random variables defined in the set $\mathcal{S}$, in which every variable F_i takes a value f_i in $\mathcal{L}$. The $\mathcal{F}$ family is called a random field. The probability that the random variable F_i takes the value f_i is denoted as $P(f_i)$, and the joint probability is denoted as $P(f)$. It is said that $\mathcal{F}$ is a Markov random field on $\mathcal{S}$ with respect to the neighboring system $\mathcal{N}$ if and only if: $P(f) > 0, \forall f \in \mathcal{F}$ and $P(f_i | f_{\mathcal{S}-\{i\}}) = P(f_i | f_{\mathcal{N}_i})$. Intuitively, this means that the label of a site only depends on the direct neighbors.

The equivalence between the Markov random field and the Gibbs distributions provides a simple way of specifying the joint probability of an MRF. A set of variables $\mathcal{F}$ is said to be a Gibbs random field (GRF) in $\mathcal{S}$ with respect to $\mathcal{N}$ if and only if it obeys a Gibbs distribution:

$$\begin{aligned} P(f) &= Z^{-1} \times e^{-\frac{1}{T}U(f)}, \\ Z &= \sum_{f \in \mathcal{F}} e^{-\frac{1}{T}U(f)}, \\ U(f) &= \sum_{c \in \mathcal{C}} V_c(f), \end{aligned} \tag{1}$$

where Z is a normalization constant called *partition function*, T is a constant called *temperature* and $U(f)$ is the *energy function* defined as a sum over the clique potential $V_c(f)$, which solely depends on the local configuration of the c clique. The equivalence between the Markov and Gibbs fields permits specification of the joint probability $P(\mathcal{F} = f)$ specifying the clique potentials, which will be defined as a function of the desired behavior. In this way the *a priori* knowledge is encoded.

To calculate the joint probability of an MRF, that is a Gibbs distribution, it is necessary to evaluate Z. As this implies adding up of all the possible configurations, the calculation is normally intractable. The explicit evaluation can be avoided in vision models based on the maximum probability.

When we have the knowledge about both prior and likelihood distributions, the best is to maximize Bayes criteria. The *maximum a priori probability* (MAP) is the most popular in MRF modeling (Geman and Geman, 1984). In the MAP formulation, the image interpretation can be defined as the following optimization problem:

$$f^* = arg \max_{f \in \mathcal{F}} P(f|d) = arg \max_{f \in \mathcal{F}} p(d|f)P(f) \tag{2}$$

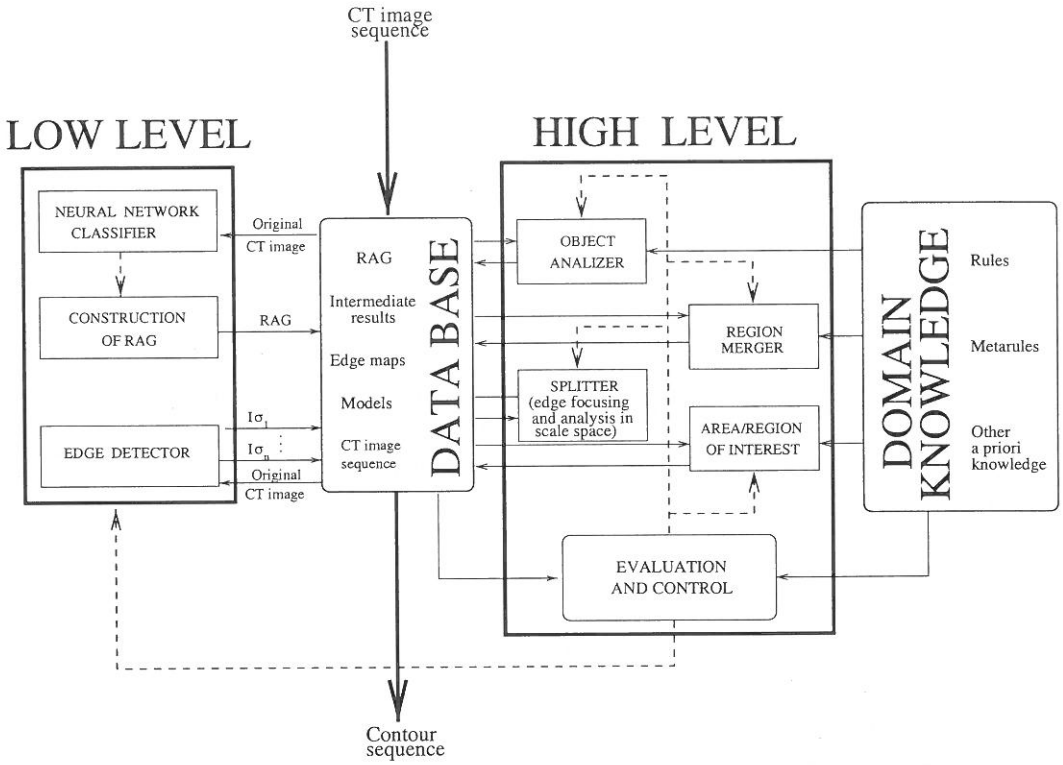

Fig. 2. Global scheme of the region growing system.

Taking into account that $\mathcal{F}$ is a MRF, this results in:

$$f^* = arg\min_f U(f|d)$$
$$= arg\min_f \{U(d|f) + U(d)\} \qquad (3)$$

In our high level image analysis, the image features are regions. A scene will be represented by means of features (d) of the regions and the relations ($\mathcal{N}$) between them. We search the configuration (segmentation) that minimizes the energy function using the simulated annealing algorithm (Kirkpatrick et al., 1983).

3. Integration of Segmentations

In the introduction, some features of the region- and edge-based segmentation methods were reported. In this section, an overview of our previous work on region growing and snake models has been made, and after comparing their performance we present our proposal of integration.

3.1. Region Growing Approach

The region-based segmentation can be improved by introducing knowledge about the domain. The rule-based systems represent this knowledge by means of a set of rules that allow them to carry out segmentation control driven by data and/or by model. We have implemented a rule-based approach for region growing whose scheme is sketched in Fig. 2. The system has two main blocks: low level (extracts low level features) and high level (performs region growing by using domain knowledge). The system has also two memories: data base (input, output, intermediate results, etc.), knowledge domain (rules, strategies, etc.). The system begins to carry out a low level presegmentation by means of a neural network classifier (Cabello et al., 1993). Then, regions and their features (shape, densitometric and relational) are organized in a region adjacency graph (RAG), where the nodes contains region features and the weighted arcs represent the size of the shared contours. After the presegmentation, the high level stage works directly over the RAG. It begins with the selection of growing kernels of bone areas and completes the recognition of the bone structures by applying rules for the merging and the division of regions. The growing process is driven by a set of fuzzy rules that embodies criteria

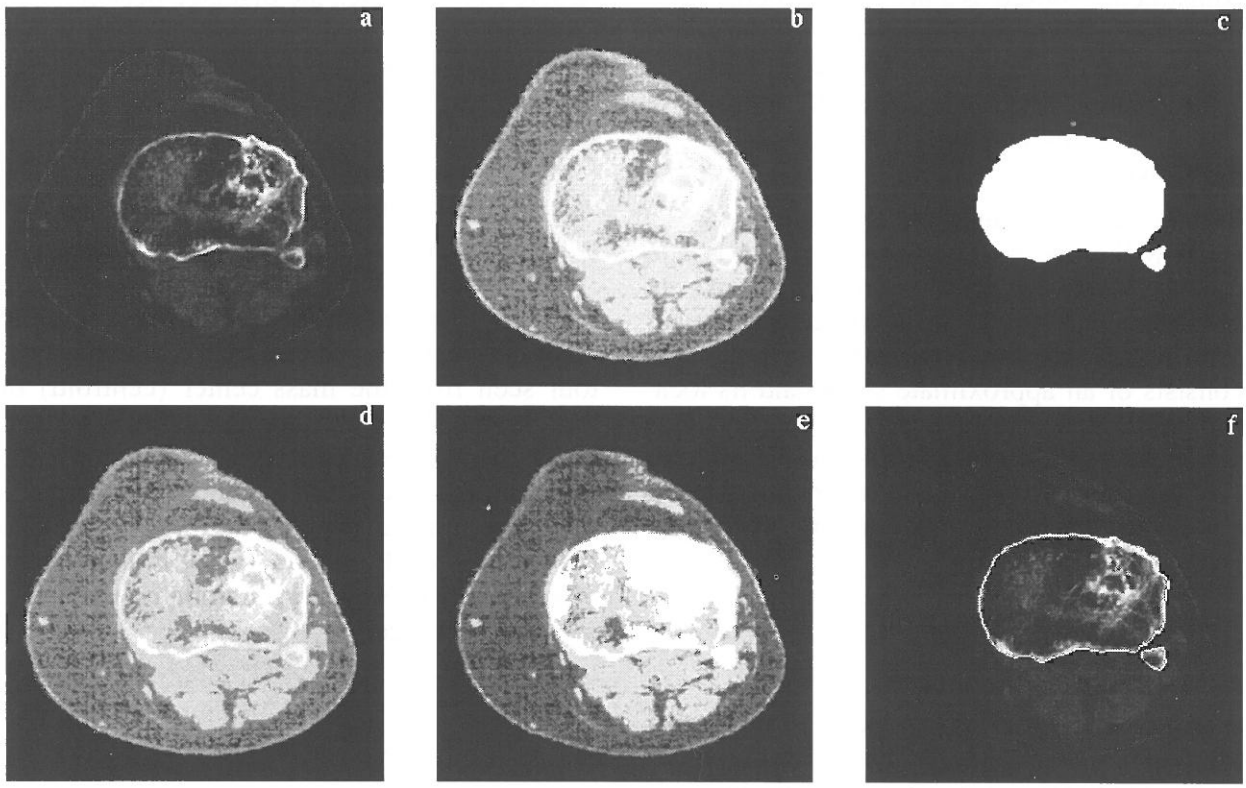

Fig. 3. (a) Original image; (b) presegmentation; (c) model; (d) growing kernels for tibia (white regions); (e) intermediate state; (f) final segmentation.

as compactness, closure, spatial closeness, and distance to a model. Given the 3D continuity of the bone structure, shape and location of bone in each slice are similar to those in the previous slice. So, the bone contour delineated in the previous slice is considered as a model for the current slice. The process starts by defining an area of interest (AOI) by means of the dilation of the model mask. Regions whose centroid are out of this area are discarded. From the remaining regions, the most dense ones are chosen as the growing kernels (the higher the intensity, the higher the probability of belonging to the bone). All these tasks are carried out by the block *Area/Region Of Interest*. The bone growing is performed by the combined action of two blocks *Region Merger* and *Object Analizer*, which decide on the the merging of neighboring regions to bone kernels, and the incorporation of new bone kernels respectively. The process iterates until a stop criterion, derived from the measurement of matching between objects and models, is achieved in the *Evaluation And Control* block. If different structures appear overlaid, then a splitting process, guided by edge information (low level), has to be carried out. Edge information is obtained combining the outputs of an edge operator with several scales ($I_{\sigma_1}, \cdots, I_{\sigma_n}$) and taking into account the shape and location of the model (constraints imposed by the knowledge on the domain). The system has a special sub-block for edge focusing and scale space analysis. A more detailed description of the overall system can be found in (Pardo et al., 1995). Fig. 3 illustrates the growing process.

3.2. Deformable Contour Model

From the edge-based methods, those that are receiving most attention are actually the deformable contour methods. One of the main reasons for their popularity is the easiness of the implementation of a mixed control strategy, bottom-up (data-driven) and top-down (model-driven). We have implemented a system of deformable contours where we introduced new energy terms which are adequate for the domain of CT images of the knee (Pardo et al., 1997). It takes the final contour of the structure in the previous slice and tries to adjust it to the contour this structure has in the actual slice. The

adjustment is posed as a process of energy minimization. Thus, it is necessary to define an energy as a function of the image data and the *a priori* knowledge, so that the minimum corresponds with the position of the real contour of the structure.

In the absence of important external forces, the snake will move in a circular shape and begin to contract towards a point. Moreover, when a set of consecutive slices is being processed, the information transferred from one slice to the next consists of an approximate shape and its location. Classical internal energy expression does not impose constraints on this knowledge. For the cases in which a good initial model is available, it is convenient to add an internal energy term:

$$\sum_{i \in v_i} \kappa(i) \left[1 - e^{-|v_i - v_i^0|^2/2\sigma}\right] \qquad (4)$$

where $\kappa(i)$ is a positive parameter, v_i^0 represents the position of the i-th vertex of the initial deformable model and σ controls the *flexibility* in the deviation with respect to this initial position. This term constrains the final contour to be near the initial contour (model).

One of the main problems related to the use of snakes is strong dependence on the initial contour. In an attempt to mitigate the problems of bad initialization, we have proposed a potential to be added to the classical terms for the gradient, intensity and the proximity to points on the edge map. The expression of the potential is:

$$P(v_i) = -\gamma \left| \nabla [G(v_i) * I(v_i)] \right| - \delta I(v_i) - \zeta e^{-d(v_i)^2} - \eta \frac{\partial}{\partial \vec{n}} I(v_i) \qquad (5)$$

where $d(v_i)$ denotes the distance between vertex v_i and the closest boundary, and $\gamma, \delta, \zeta, \eta$ are positive constants. The fourth term causes the snake to shift towards the external contour in the case of structures with a double contour (cortical bone), and towards the contour of the *closest* structure in the case of proximity to other structures. Here $\vec{n}$ represents the normal to the snake. When the structure has a double contour, this new potential term presents the minimum value in the exact position of the external contour seen from the mass center (centroid) of the curve. When the initial model is located between two close structures, for example the tibia and the fibula, this potential term attracts the curve towards the contour that is closest to the centroid of the snake. Fig. 4 illustrates the effect of new energy terms compared with classical implementation.

3.3. Comparison

In the processing of CT images of the knee both methods give, in general, good results with similar quality. However, in slices with low quality of the cortical bone or injuries, the segmentations can be defective. With the objective in mind to minimize the error of the automatic segmentation, we propose an integration scheme of both complementary methodologies. An advantage of the snake approach over teh region-based system is a better precision in the location of contours, as shown in Fig. 5. On the contrary, snakes are more sensitive to noise and fine textures of the trabecular bone. The region growing method is based on the features of the

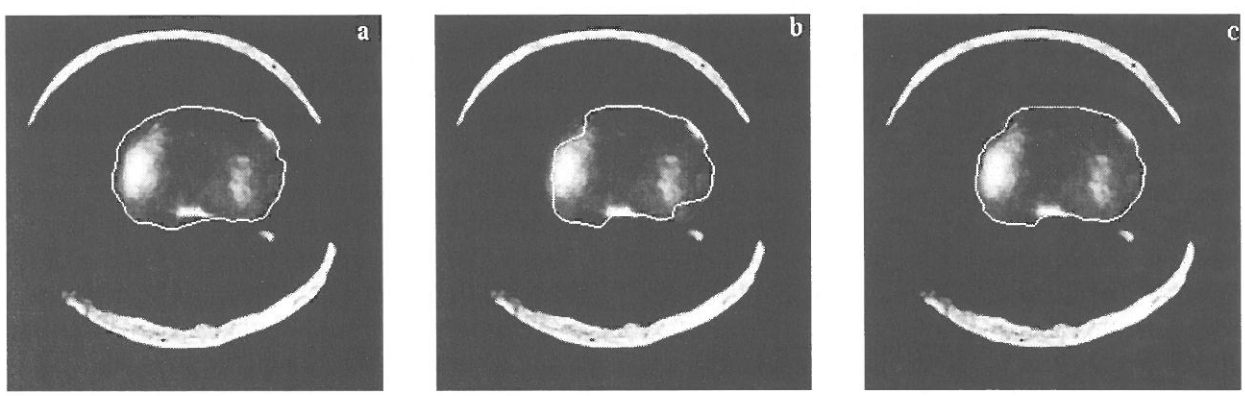

Fig. 4. (a) Initial contour; (b) final contour obtained with a classical snake model; (c) result attained with the new energy terms.

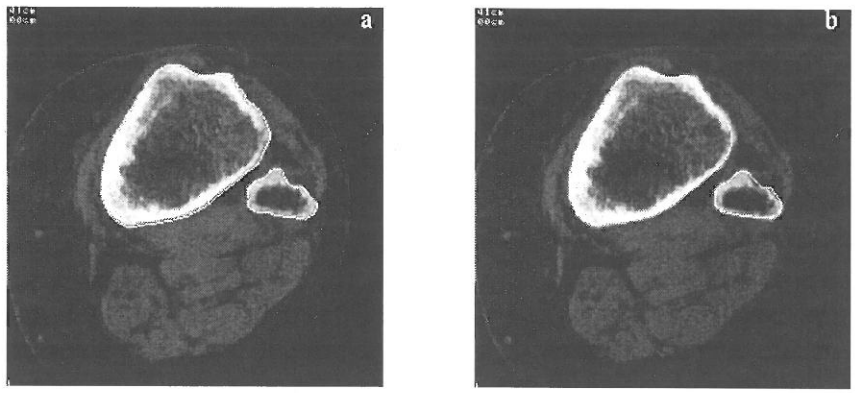

Fig. 5. Segmentations by means of: (a) region growing; (b) deformable contours.

pixel neighborhood, more than on the local features of such a pixel. This provokes expansion of the bone segment outside of its real limits as observed in Fig. 5a, and that narrow regions are lost as Fig. 6a illustrates.

On the other hand, the region growing system depends less on the initial model than on the deformable contour model. This fact is revealed in Fig. 7, where two slices have been randomly chosen and the segmentations have been carried out using different contour models. These models are the real contours of the same structure in various adjacent slices. When an important difference between adjacent slices exists, segmentation by means of deformable contours is unreliable. It is for this reason that a robust segmentation cannot be exclusively based on them in spite of their good properties.

3.4. Integration

To carry out the most reliable segmentation we have proposed integration of both methods' results. For this integration we employ the MRF model, which has received special attention as an integration scheme of constraints for the interpretation of images (Modestino and Zhang, 1992; Kim and Yang, 1996). Although the majority of published works related to the MRF model deal with pixels as sites for labeling, the natural extension to image structures with a more abstract level, as regions, can be reached.

The integration system considers those parts of the original image which are classified as bone in both systems as secure bone regions. It also considers as a secure background region the one that in both cases received this classification. The integration system will not modify classification of such regions, but will only work on the regions that have received a distinct classification in each segmentation system. These image areas will be partitioned as in the low level presegmentation. The scheme based on the MRF model will decide on the incorporation of these regions (classified as bone by only one of the segmentation systems) to the bone or to the background. Fig. 8 shows the input to the integration system for the two segmentations in Fig. 6. Level 255 represents secure bone zone,

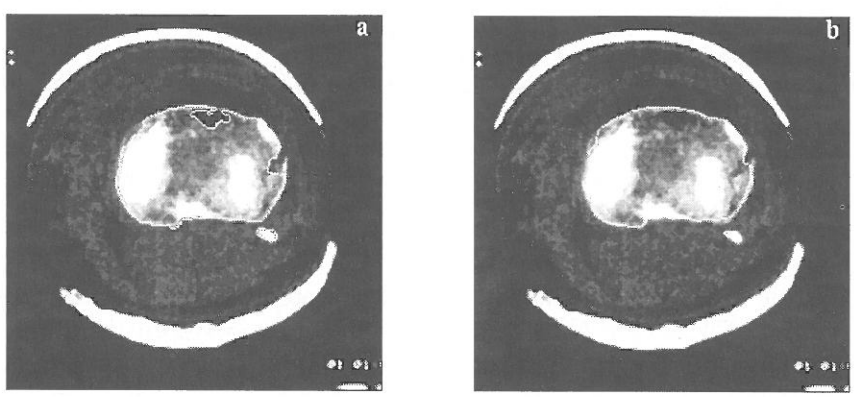

Fig. 6. Segmentation by: (a) region growing, (b) deformable contours.

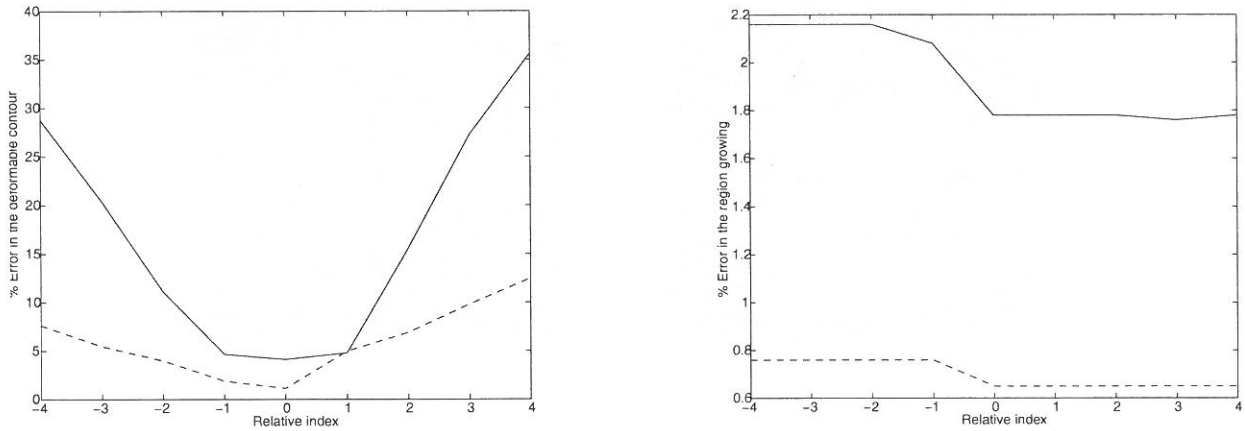

Fig. 7. Dependency of the regiong growing and deformable contour methods with the initial model. The horizontal axis represents the relative position of the slices in the sequence whose final contours have been taken as initial contours. The vertical axis represents the % of error with respect to a manual segmentation. Continuous and dotted lines represent two different cases.

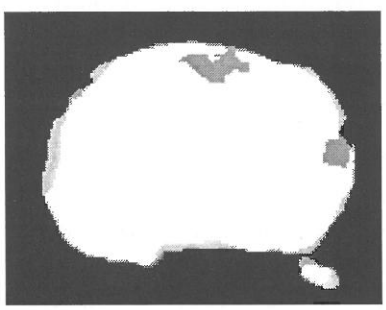

Fig. 8. Map of input regions to the integration system. The system will decide on the labeling of the regions with a gray value more than 0 or less than 255.

0 represents background, and the intermediate levels represent regions to label. The regions considered as secure bone receive a label with value 2 for the tibia and 3 for fibula. The secure background regions receive a label with value 0. Initially, the rest of the regions are randomly labeled as bone (label 1) or background (label -1). The optimization of the labeling is estimated through a unified energy function.

In our application, the sites correspond to the set of N regions $\mathcal{R} = \{R_1, \ldots, R_N\}$ as commented before. From these a graph $\mathcal{G} = \{\mathcal{R}, \mathcal{E}, \mathcal{D}\}$ is defined, where $\mathcal{E}$ represents the set of edges that connect the regions, and $\mathcal{D} = \{d_1, d_2\}$ represents the set of features: of the region (d_1), or of the relation with neighboring regions(d_2). With this graph it is possible to define a neighborhood system $\mathcal{N} = \{N_i | \forall i \in \mathcal{R}\}$, where N_i is the set of neighbors of R_i. Two sites (regions) are considered neighbors if they share an edge. The set of labels is $\mathcal{L} = \{3, 2, 1, 0, -1\}$ ={tibia, fibula, probable bone, background, probable background}. The integration problem is formulated as the problem of assigning an $\mathcal{L}$ label to each one of the $\mathcal{R}$ sites, or, equivalently as a set of random variables $\mathcal{I} = \{I_1, \ldots, I_N\}$ defined over $\mathcal{R}$. $\mathcal{I}$ is the random field, and $I_i \in \{-1, 1\}$ is the random variable associated with R_i. $\mathcal{I}$ is the MRF model over $\mathcal{G}$ with respect to the neighborhood system $\mathcal{N}$.

The optimal segmentation (configuration) is evaluated over the energy function that is now defined:

$$U(I) = \sum_{i \in \mathcal{R}} V_1(I_i) + \sum_{i \in \mathcal{R}} \sum_{i' \in \mathcal{N}_i} V_2(I_i, I_{i'})$$
$$+ \sum_{i \in \mathcal{R}} V_1(d_1 | I_i) + \sum_{i \in \mathcal{R}} \sum_{i' \in \mathcal{N}_i} V_2(d_2(i, i') | I_i, I_{i'})$$

where V_1 refers to the energy functions that only take into account labels or features of individual regions (d_1), and V_2 represents the energy functions dependent on the relation between two regions (d_2).

In our application the labels with value 0 (secure background), 2 (secure fibula) and 3 (secure tibia) do not change. The regions with these labels are included in the region adjacency graph, but are only used to evaluate relating features with the regions in analysis.

The potentials are defined in such a way that connection between different structures (tibia and fibula) is avoided, the regular shape of the bone is favoured, and they have the tendency to label as background those regions which are far from the secure bone. These last regions

were generated by growing regions and represent transition zones and appear as a series of parallel and narrow regions. It is also necessary to eliminate gaps in the bone. Then labeling must favour the bone label if all its neighbors are labeled in the same way. It also takes into account the gray level for the guidance of the integration. The (d_1) features of individual regions that are employed here are: perimeter (P), average gray level (ρ) and its variance (σ). The relation properties used are: adjacency to the background $(\text{Is\_Ady\_B} \in \{1, 0\})$, connectivity of different structures $(\text{Con\_D\_St} \in \{1.0\})$, shared perimeter (Per_i) with each neighbor $(R_i \in N_i)$, and the number of neighbors (NN). These features are represented in Table 1. The clique potentials should represent the afore mentioned constraints. We have constructed an energy function with the following clique potentials:

$$V_1(I_i) = 0 \tag{6}$$

$$V_2(I_i, I_{i'}) = 0 \tag{7}$$

$$V_1(d_1(i)|I_i) = \Lambda I_i \text{Con\_D\_St}(i) - \lambda I_i \frac{\rho_i + \sqrt{\sigma_i} - \rho_b}{\rho_b} \tag{8}$$

$$V_2(d_2(i, i')|I_i, I_{i'}) = \chi I_i \Theta_U\left(\frac{(I_{i'}+1)\text{Per}_{ii'}}{\text{P}_i} + \frac{\epsilon_1}{NN}\right) - \psi I_i \text{Is\_Ady\_B}(i) \Theta_{\epsilon_2}\left(\frac{(I_{i'}-1)\text{Per}_{ii'}}{\text{P}_i} + \frac{\epsilon_3}{NN}\right) - \xi I_i\left(\frac{(I_{i'}+1)\text{Per}_{ii'}}{2\text{P}_i} - P_{th}\right) \tag{9}$$

Θ_U is the Heavisade function centered on zero, it takes value 1 in arguments higher than zero and 0 in the others. The function $\Theta_{\epsilon_2}(\theta)$ takes value 1 if the argument is higher or equal to ϵ_2 and 0 in the other cases. $\Lambda, \lambda, \chi, \psi, \xi$ are positive constants. The term in Λ tries to avoid merging between different structures. The term in λ favours the inclusion, as part of the bone, of the regions with a density higher than the ρ_b threshold, and as part of the background in opposite cases. The term in χ favours the inclusion, as part of the bone, of regions where the majority of its neighbors have this label. The term in ψ has the tendency to eliminate from the bone area those regions adjacent to the background and with a small or no connection to the bone label regions. Finally, the term in ξ promotes elimination of concavities (assigning bone label) whose adjacency with the bone exceeds a Per_{th} threshold. Table 2 specifies the meaning of each energy term and the values

Features (d_1)	Definition
Area	A_i = *size of the region* R_i
Perimeter	P_i = *size of the perimeter of the region* R_i
Average gray level	$\rho = \frac{1}{A_i} \sum_{(x,y)\in R_i} I(x, y)$
Standard deviation of gray levels	$\sigma = [\frac{1}{A_i} \sum_{(x,y)\in R_i} (I(x, y) - \rho_i)^2]^{1/2}$

(a)

Features (d_2)	Definition
Background adjacency	$Is\_Ady\_B(i) = \begin{cases} 1 & \text{if } \exists i' \in N_i \text{ such that } I_{i'} = 0 \\ 0 & \text{otherwise} \end{cases}$
Connect different structures	$Con\_D\_St(i) = \begin{cases} 1 & \text{if } \exists j, k \in N_i \text{ such that } I_j = 2 \text{ and } I_k = 3 \\ 0 & \text{otherwise} \end{cases}$
Shared perimeter	Per_{ij} = *size of the contour between regions* R_i *and* R_j
Number of neighbors	NN = *number of adjacent regions*

(b)

Table 1. Definition of Features: (a) for single region, (b) for relationship.

Weight	Meaning of the Weighted Term	Degree of Magnitude
Λ	Avoid the connection between regions of different structures	∞
λ	Promote bone labeling at high densities and background labeling at low densities	1.0
χ	Promote homogeneity in labeling	1.0
ψ	Promote background labeling if regions are found to be distant from bone labeled regions	1.0
ξ	Avoid the formation of cavities in the bone	1.0

(a)

Function	Definition
$Theta_U$	$\Theta_U(\theta) = \begin{cases} 1 & \text{if } \theta \geq 1 \\ 0 & \text{otherwise} \end{cases}$
Θ_{ϵ_2}	$\Theta_{\epsilon_2}(\theta) = \begin{cases} 1 & \text{if } \theta \geq \epsilon_2 \\ 0 & \text{otherwise} \end{cases}$

(b)

Parameter	Value
ϵ_1	0
ϵ_2	0.1
ϵ_3	0
P_{th}	0.6

(c)

Table 2. Definition of: (a) energy terms, (b) functions; (c) parameter values.

given to all parameters used. These parameters were heuristically determined considering a large set of knee CT images. We found that their values are not critical, it is enough that Λ is much greater (about 2 degrees of magnitude) than other weights, and these can take the same value. Parameters ϵ_2 and P_{th} represent what we understand by the limits of small and large shared contours between regions, respectively. In our application, we found that 0.1 and 0.6 are the best values. These values were used in the processing of all the CT image sequences regardless of particular imaging conditions. Thus they do not need to be tuned for each particular case.

For the optimization of the labeling the MAP criteria are used together with the simulated annealing algorithm. The regions that, after the optimization process, have the label 0 or -1 are considered to be background, and those that have the label 1, 2 or 3 are considered to be the bone.

4. Results and Conclusions

The integration process is carried out to improve the location of the exterior contours of the structures of interest. This process takes the segmentations given by the region growing system and the snake based approach as inputs. When the two methods give a tight segmentation, the integration approximates more to the segmentation of the deformable models, as they usually offer a better location of the edges. This is seen in Fig. 9a, which shows the result of the integration of the segmentations in Fig. 5.

Another example of the performance of our integration system is the one shown in Fig. 9b for the segmentation of Fig. 6. This corresponds to an image where two injuries appear in the tibial plateau. These injuries correspond to the zones with a higher gray level inside the tibia. They

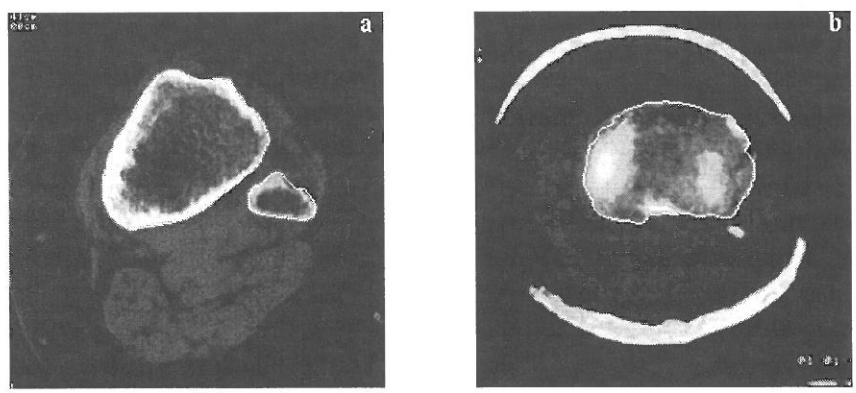

Fig. 9. Results of the integration of the segmentations of: (a) Fig. 5, (b) Fig. 6.

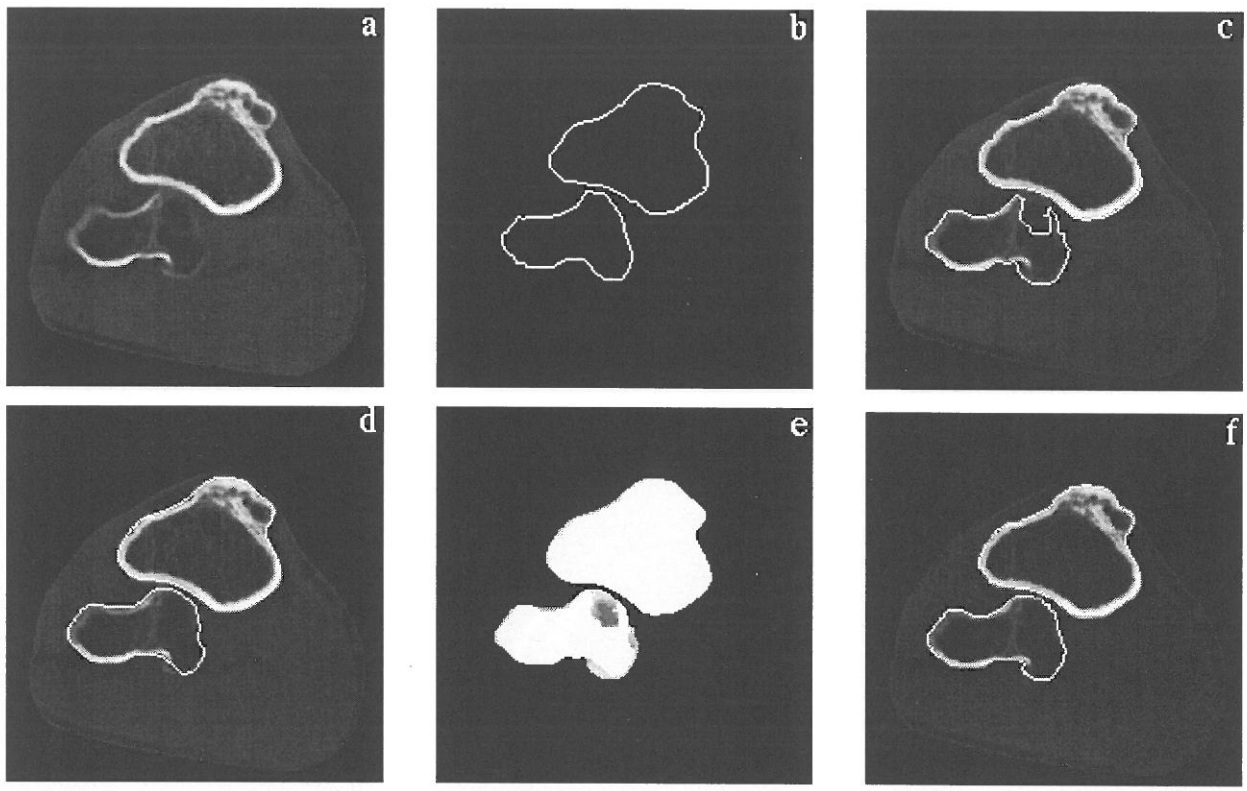

Fig. 10. (a) Original image; (b) model; (c) segmentation by region growing; (d) segmentation by snakes; (e) input to integration module; (f) result of integration.

were provoked by a fracture caused by a bone loss effect. Low quality of the cortical bone makes the transitions of gray levels between the tibia and the muscle much smoother than these that exist around the injuries. As a consequence, the region-based segmentation does not always detect presence of the cortical bone owing to the narrowness of such a bone and its low density. Another consequence can be that deformable contours are attracted by the contour of one of the injuries more than by the contour between bone and muscle. The integration scheme combines both results to offer a better segmentation as shown in Fig. 9b.

A very illustrative example of the performance of our approach can be seen in Fig. 10. In Fig. 10a an image of tibia and fibula appears, with a considerable bone loss in the fibula. It makes the region growing and deformable contour processes delineate the fibula unaccurately (Fig. 10c-d). Fig. 10e shows the differences between the two segmentations, and Fig. 10f contains the result of the integration.

In parts farther away from the proximal end of the knee, where the difference between slices is small and the cortical bone is wide and dense, the integration provokes a slight adjustment of the contours location. In the proximal end, the distance between tibia and fibula is reduced, the width of the cortical bone decreases and the injuries appear. In this part the segmentation is more complex and the integration provokes more notable improvements, as shown in Fig. 10. In Fig. 11 we can see a new example of the application of the integration system in the proximal zone. In this case the region growing system initially merged the tibia and fibula. The division process separated both structures, but also eliminated part of the cortical bone of the tibia, Fig. 11a. On the other hand, the deformable contour adjusted to the internal contour of the cortical bone owing to the initial model being situated in the interior of the bone, Fig. 11b. The integration of both segmentations produces a better result as can be observed in Fig. 11c.

Fig. 12 shows an example of neighboring structures with a injury in-between them. In that case, region growing cannot achieve a complete separation between the tibia and fibula as shown in Fig. 12a; and with the deformable contour approach it is necessary to impose an exces-

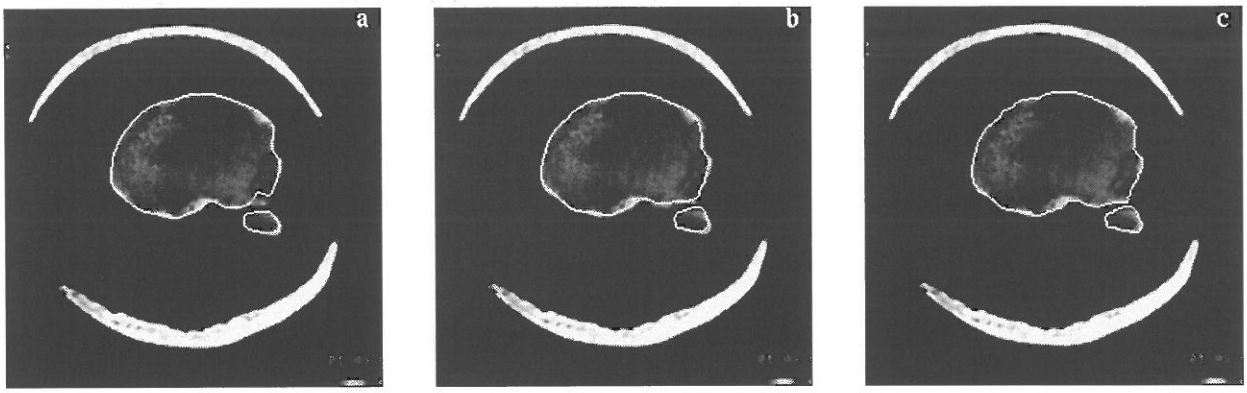

Fig. 11. (a) Segmentation by: region growing, (b) snake; (c) integration.

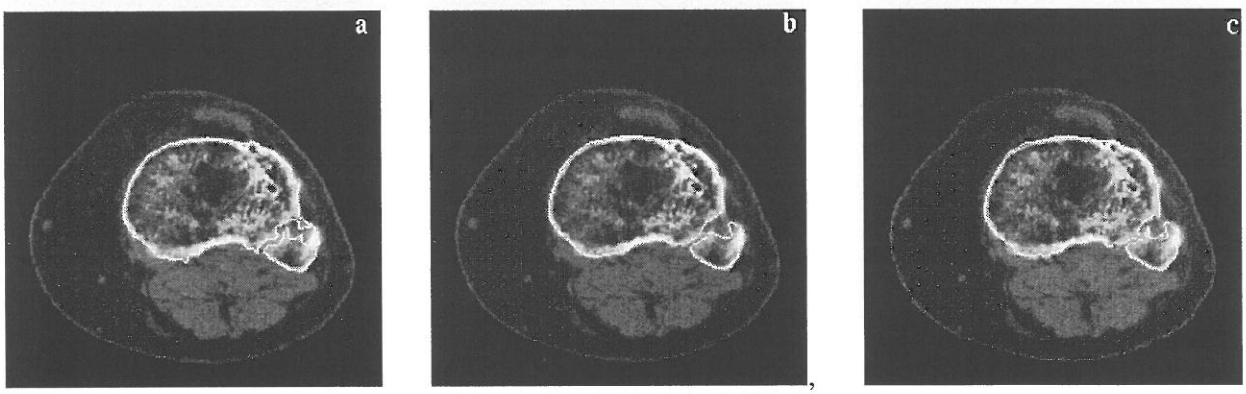

Fig. 12. Segmentation of neighboring structures by: (a) region growing; (b) snakes; (c) integration.

sive smoothness to avoid the contact between the two structures. By means of an integration scheme it is possible to attain a more precise segmentation, Fig. 12c.

Finally, in Fig. 13 we show the segmentations of 12 intermediate slices of a CT image sequence composed of 76 slices.

As we have commented on before, both the region growing and the snake based methods produce good segmentation in the majority of cases. However, none of these methods is foolproof. When injuries, deformations or bone loss appear, the similarity between the texture of certain bone tissues and the muscle increases, and borders become diffused and disconnected. So, the quality of the segmentations strongly depends on the values of the segmentation parameters. Integration of different segmentation strategies is highly recommended to find the most probable contour location, and to avoid the need of a precise tuning of segmentation parameters, because definite decisions are made by the integration scheme. In this way, errors in individual segmentations can be detected and corrected. On the other hand, we found that values of the parameters involved in the integration process are not critical, and the heuristic values formerly shown work well in all considered cases. With our integration system we overcome several inconveniences presented by individual modules. In this way we obtain a more robust segmentation method.

The method has been used in the segmentation of four CT image sequences, in total more than 300 images have been analyzed, and the speed of segmentation was between 1 and 1.5 minutes per slice in a SUN SPARC 10. Since the main motivation for medical image segmentation is to automate all or part of manual segmentation, it was important to compare the results of our algorithm with those of manual segmentation. Two medical experts carried out the segmentation of one image sequence, taking, in average, 5 minutes per slice. After comparing the two segmentations with the one offered by our method, we found that, generally, the discrepancy between the manual segmentations is greater than the discrepancy between the automatic segmentation and each of the manual ones.

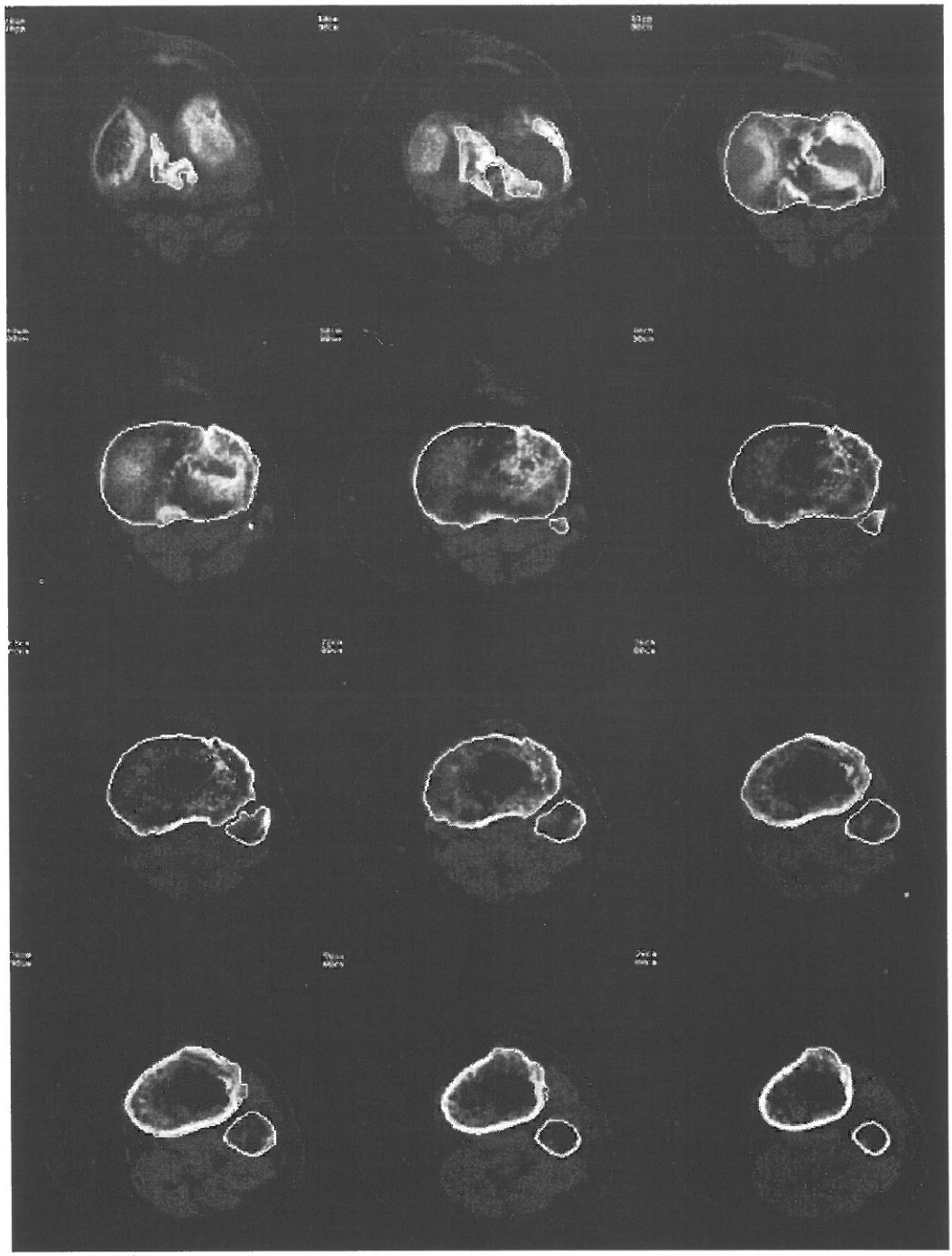

Fig. 13. Intermediate slice segmentations in a CT image sequence of 76 slices.

There still remains work to be carried out in obtaining potential terms that make the integration strategy better, and in the development of a reliable evaluation system of the segmentation results. In this way the global segmentation system could be based on one of the modules and thus would decide whether it is needed to incorporate additional knowledge or not. In the case new information is needed, the system would use the other module and would finally integrate the results.

References

[1] S. ARITAN, P. DABNICHKI AND R. BARTLETT, Program for generation of three-dimensional finite element mesh from magnetic resonance imaging scans of humans limbs, *Medical Engineering and Physics*, 19(1997), 681–689.

[2] M. S. BROWN, M. F. MCNITT-GRAY, N. J. MANKOVICH, J. G. GOLDIN, J. HILLER, L. S. WILSON AND D. R. ABERLE, Method for segmenting chest CT image data using an anatomical model:

preliminary results, *IEEE Transactions on Medical Imaging*, 16(1997), 828–839.

[3] D. CABELLO, M. G. PENEDO, S. BARRO, J. M. PARDO AND J. HERAS, CT image segmentation by self-organaizing learning, In *Lecture Notes in Computer Science: New trends in neural computation* (J. Mira, J. Cabestany and A. Prieto, Eds.) (1993) pp. 651–656, Spring–Verlag.

[4] A. CHAKRABORTY, L. H. STAIB AND J. S. DUNCAN, Deformable boundary finding in medical images by integrating gradient and region information, *IEEE Transactions on Medical Imaging*, 15(1996), 859–870.

[5] C.-C. CHU AND J. K. AGGARWAL, The integration of image segmentation maps using region and edge information, *IEEE Transactions on Pattern Analysis and Machine Intelligence*, 15(1993), 1241–1252.

[6] P. DARIO, C. PAGGETI, T. CIUCCI, D. BERTELLI, B. ALLOTA, M. MARCACCI, M. FADDA, S. MARTELLI AND D. CARAMELLA, A system for computer-assisted articular surgery, *Journal of Computer Aided Surgery*, (1996), 48–49.

[7] A. P. DHAWAN AND L. ARATA, Knowledge-based 3D analysis from 2D medical images, *IEEE Engineering in Medicine and Biology*, 10(1991), 30–37.

[8] S. GEMAN AND D. GEMAN, Stochastic relaxation, Gibbs distribution, and Bayesian restoration of images, *IEEE Transactions on Pattern Analysis and Machine Intelligence*, 6(1984), 721–741.

[9] M. KASS, A. WITKIN AND D. TERZOPOULOS, Snake: active Contour models, *International Journal of Computer Vision*, 1(1988), 321–331.

[10] J. H. KEYAK, M. G. FOURKAS, J. M. MEAGHER AND H. B. SKINNER, Validation of an automated method of three-dimensional finite element modelling of bone, *Journal of Biomedical Engineering*, 15(1993), 505–509.

[11] I. Y. KIM AND H. S. YANG, An interpretation scheme for image segmentation and labeling based on Markov random field model, *IEEE Transactions on Pattern Analysis and Machine Intelligence*, 18(1996), 69–73.

[12] S. KIRKPATRICK, C. D. GELATT AND M. P. VECCHI, Optimization by simulated annealing, *Science*, 220(1983), 671–680.

[13] S. Z. LI, *Markov Random Field Modeling in Computer Vision*, Springer–Verlag, Tokio, 1995.

[14] T. MCINERNEY AND D. TERZOPOULOS, Topologically adaptable snakes, Presented at the *Proceedings ICCV'95*, (1995), Berlin, Germany.

[15] J. W. MODESTINO AND J. ZHANG, A Markov random field model-based approach to image interpretation, *IEEE Transactions on Pattern Analysis and Machine Intelligence*, 14(1992), 606–615.

[16] R. MÜLLER AND P. RÜEGSEGGER, Three-dimensional finite element modelling of non-invasively assessed trabecular bone structures, *Medical Engineering and Physics*, 17(1995), 126–133.

[17] J. M. PARDO, D. CABELLO, M. J. CARREIRA, M. G. PENEDO AND J. HERAS, Knowledge-based CT image analysis: automatic 3D shape reconstruction of bones, In *Proceedings of the Second Asian Conference on Computer Vision*, (1995) Nayang Technological University, Singapore.

[18] J. M. PARDO, D. CABELLO, AND J. HERAS, A snake for model-based segmentation of biomedial images, *Pattern Recognition Letters*, 18(1997), 1529–1538.

[19] T. PAVLIDIS AND Y.-T. LIOW, Integration region growing and edge detection, *IEEE Transactions on Pattern Analysis and Machine Intelligence*, 12(1990), 225–233.

[20] E. PEPINO, M. CESARELLI, F. DI SALLE, A. MOSCA AND M. BRACALE, Preliminary notes on the conversion of three-dimensional images of bones into CAD structures for the pre-operative planning of intertrochantheric osteotomies, *Medical and Biological Engineering and Computing*, 31(1993), 529–534.

[21] M. SONKA, W. PARK AND E. A. HOFFMAN, Rule-based detection of intrathoracic airway trees, *IEEE Transactions on Medical Imaging*, 15(1996), 314–326.

[22] H. TEK AND B. B. KIMIA, Volumetric segmentation of medical images by three-dimensional bubbles, *Computer Vision and Image Understanding*, 65(1997), 246–258.

Received: August, 1998
Revised: June, 1999
Accepted: September, 1999

Contact address:
X. M. Pardo
Campus Universitario
15706 Santiago de Compostela
Galicia
Spain
e-mail: pardo@dec.usc.es

D. Cabello
Campus Universitario
15706 Santiago de Compostela
Galicia
Spain
e-mail: diego@dec.usc.es

J. Heras
Servicio de Cirurxía Ortopédica
Complexo Hospitalario Universitario
Santiago de Compostela
Galicia
Spain

XOSÉ M. PARDO was born in 1968 in Malpica (A Coruna), Spain. He recived the B.Sc. and Ph.D. degres in Physics in 1991 and 1998, respectively, from the University of Santiago de Compostela. Since November 1993 he has been an assistant professor at the University of Santiago de Compostela, where he is teaching courses related to computer science and image processing. His current research interest is medical image analysis and computer graphics, including stochastic labeling, segmentation by deformable models and solid modeling.

DIEGO CABELLO received the Ph.D. in Physics from the University of Santiago de Compostela in 1984. Present appointment: Professor of Electronics and dean of the Faculty of Physics of the University of Santiago de Compostela. His research interest is in microelectronic implementation of artificial neural networks for early vision, and development of intelligent systems for image understanding.

JOAQUÍN HERAS was born in 1954 and received the B.Sc. in Medicine from the University of Salamanca, Spain in 1979. Present appointment: Staff member and predoctoral research in the Orthopaedic Surgery and Trauma Dpt. of the General Hospital of the University of Santiago de Compostela. His research interest and lines are: artificial intelligence and expert systems development in total joint replacement domain, artificial neural networks (applications in CT and radiographic image analysis) and biomaterials and bone-tissue interactions. Clinical special interest in joint reconstruction.